Analytica Chimica Acta xxx (2017) 1–8

Contents lists available at ScienceDirect

Analytica Chimica Acta

journal homepage: www.elsevier.com/locate/aca

Double labelling of intracellular mitochondria and nucleolus using thiophene pyridium salt with high quantum yield as biosensor and its application in stimulated emission depletion nanoscopy

Xiaohe Tian [a, *], Hui Wang [c], Qiong Zhang [b], Mingzhu Zhang [b], Yingzhong Zhu [b], Yan Chen [a], Jieying Wu [b], Yupeng Tian [b, d, **]

[a] School of Life Science, Anhui University, Hefei 230601, PR China
[b] Department of Chemistry, Anhui Province Key Laboratory of Chemistry for Inorganic/Organic Hybrid Functionalized Materials, Anhui University, Hefei 230601, PR China
[c] Department of Chemistry, Wannan Medical College, Wuhu 241002, PR China
[d] State Key Laboratory of Coordination Chemistry, Nanjing University, Nanjing 210093, PR China

HIGHLIGHTS

- A small water-soluble pyridium based compounds with two-photon activity.
- High sensitivity and selectivity against RNA.
- This probe render double labelling of mitochondria and nucleolus with superb photo-stability and non-invasiveness.
- Its application of revealing mitochondrial and nucleolar ultrastructure under STED was displayed.

GRAPHICAL ABSTRACT

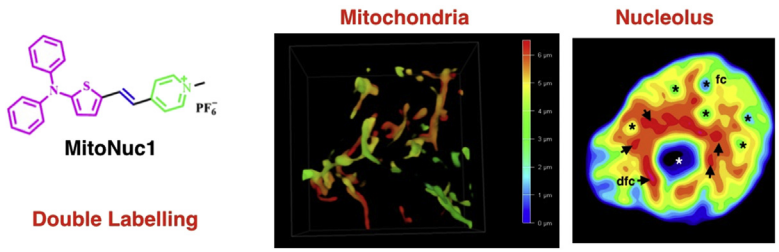

ARTICLE INFO

Article history:
Received 1 October 2017
Received in revised form
4 December 2017
Accepted 11 December 2017
Available online xxx

Keywords:
Double-labelling
RNA
Mitochondrial
Bioimaging
STED

ABSTRACT

Probe for dual-site target distinct subcellular compartments from cytosol and nucleus is an attractive approach, however, which was scarcely reported. Herein, a series of small-molecular thiophene pyridium salt derivatives (**MitoNuc1-4**) possessing water-soluble, high quantum yield and two-photon activity were rationally designed, and their structures were crystallographic confirmed. Systematic photophysical and biological imaging property investigations were carried out for them. It was found that **MitoNuc1-4** exhibit two-photon absorption properties in the near infrared region, and **MitoNuc1** has membrane permeability and cationic nature, rendering it to be double labelling of mitochondria and nucleolus in living cells with superb photo-stability and non-invasiveness. It also demonstrated that **MitoNuc1** in living cells can monitor mitochondrial division in real time and revealed nucleolar ultrastructure under stimulated emission depletion nanoscopy.

1. Introduction

Labelling subcellular organelles in living samples under laser microscopy are of great importance and have become a universal strategy in biological related research [1–3]. In particular, its power

* Corresponding author.
** Corresponding author. Department of Chemistry, Anhui Province Key Laboratory of Chemistry for Inorganic/Organic Hybrid Functionalized Materials, Anhui University, Hefei 230601, PR China.
E-mail addresses: xiaohe.t@ahu.edu.cn (X. Tian), yptian@ahu.edu.cn (Y. Tian).

https://doi.org/10.1016/j.aca.2017.12.033
0003-2670/

has been further extended to super resolution (SR) fluorescence microscopy [4,5], such as stimulated emission depletion (STED) microscopy (or nanoscopy) [6,7], which offers the resolution down to hundreds nanometers (e.g. ~ 200 nm for green fluorescent protein, GFP). Whereas SR applications were somehow limited in fixed or transfected samples, as well as suffering the risk of alternation the very ultrastructure using concentrated markers during such process [8].

In living system, individual organelle (e.g. mitochondria, ribosome, nucleus and nucleolus) is given priority to specific roles, whereas there is little doubt that each of them are inextricably linked either in physical or functional manner. For instance, nucleolus, ribosomes, endoplasmic reticulum and mitochondrial etc. Are all involved and closely correlated during the course of synthesising quaternary structural protein from single amino acid [9]. It is known that mitochondria play essential roles in many biological functions and service as a 'power house' for other organelles; while nucleolus functions as storeroom of nuclear RNA. It is believed that the nucleolus number and size directly attribute for intracellular protein synthesis capability (or activity) [10]. In order to study the complexities and the coordination of biological process involving mitochondria and nucleolus as the above mentioned in living system, it is generally considered that double or even triple labelling of distinct organelles are necessary. Thus, small-molecule imaging probes are attractive and versatile tools for studying living system due to their mild toxicity, easy penetration and sensitive detection. Consequently, several efforts were assigned to such purpose and a number of them became commercially available [11,12]. Due to diverse nature of each intracellular component, varied targeting moieties were well developed. For example, triphenylphosphonium could be accumulated in mitochondria, and morpholine could specifically label acidic lysosomes [3,13]. However, double or triple labelling of each subcellular organelles require multiple steps of staining or washing, subsequently, introduce unexpected toxicity, cell stress and signal crosstalk. One probe for multiple organelles labelling is definitely ideal, yet rarely existed.

Within varied developed fluorescent probes, pyridinium salts, with both cationic and anionic units, have been extensively investigated in the nonlinear optical (NLO) materials, as well as considered to be potential candidates for two-photon microscopy [14–18]. Pyridinium salt derivatives possess an overall positive charge, which facilitates the permeation through the plasma membrane into mitochondria of cells and have a high tendency to genetic substances including DNA and RNA [19,20]. However, a survey of recent literature revealed that pyridinium salt derivatives possess low quantum yield [21–23], which may not favour for biological laser microscopy and its extended SR utilities. Furthermore, thiophene derivatives have also attracted much attention due to the rich electronic feature of the thiophene moiety [24,25]. Thiophene unit acts as a π-conjugated bridge, which owns higher stability than the double bond, and higher electron delocalization than benzene. Therefore, it can be used to construct molecular optoelectronic functional materials. It was proposed that the derivatives containing a thiophene unit should result in large molecular hyperpolarizability and charge transfer, which are necessary for the photophysical properties and NLO responses [26,27].

Bearing these in mind, pyridium based biosensor **MitoNuc1-MitoNuc4** have been rationally designed and synthesised (Scheme 1 and Fig. S1), its double labelling purpose would be achieved *via* following considerations: (1) The triphenylamine/diphenylamine thiophene group and ethyoxyl moiety acts as donor (D) and N-methyl pyridinium moiety acts as acceptor (A) to form a D-π-A system, resulting in strong and concomitant optimization of optical performances [20]. (2) Ethyoxyl was also attached to the triphenylamine group to enhance its electron-donating ability and improve solubility of the compounds. (3) The pyridium salts, PF_6^- anion, as well as thiophene group should make the designed compounds to be good water-soluble, photostability and biocompatibility. The results confirmed that compound **MitoNuc1** displayed good water solubility and relative high quantum yield, and possessed high affinity with RNA *in vitro*. Further *in cellulo* studies observed mitochondria and nucleolus double labelling under confocal microscopy with superb biocompatibility and photonstability. We further showed **MitoNuc1** is capable of displaying mitochondria and nucleolus ultrastructure in living system under stimulated emission depletion (STED) nanoscopy. Such outcome offered valuable tools as intracellular double labeling probe to monitor mitochondrial and nucleolar dynamic functions simultaneously in living system.

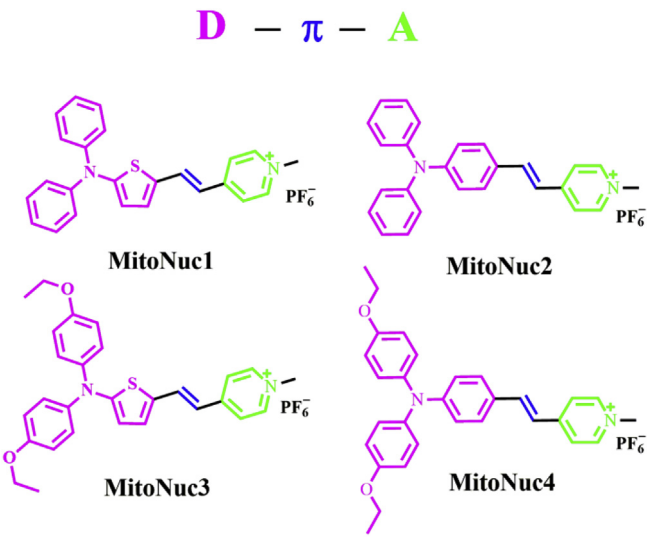

Scheme 1. The title compounds of **MitoNuc1**, **MitoNuc2**, **MitoNuc3 and MitoNuc4.**

2. Experimental sections

2.1. Materials and apparatus

All chemicals and solvents were dried and purified by the standard methods. ^{1}H NMR and ^{13}C NMR spectra were carried out on a Bruker 400 Ultrashield spectrometer using DMSO-d_6 as the solvent. MALDI-TOF mass spectra were recorded on a Bruker Autoflex III Smartbeam. IR spectra were obtained on a Nicolet FT-IR 870 SX spectrophotometer with KBr pellets.

UV-*vis* absorption spectra and one-photon fluorescence spectra were carried out on a SHIMADZU UV-3600 spectrophotometer and HITACHI F-7000 spectrophotometer, respectively. The two-photon cross-section was measured by two-photon excited fluorescence method and Z-scan method at femtosecond laser pulse and Ti: sapphire system (680–1080 nm, 140 fs) as the light source.

2.2. Synthesis

The corresponding aldehyde derivatives [28–31] (10 mmol) and M (2.35 g, 10 mmol) were dissolved in 50 mL ethanol, and then added 5 drops piperidine, refluxed for 8 h. The mixture was cooled to room temperature and filtered, washed twice with ethanol. Pure solid was collected. Single crystals of **MitoNuc2-MitoNuc4** suitable for X-ray diffraction analysis were obtained.

MitoNuc1: Yield: 78%, Mp: 220 °C. ^{1}H-NMR (DMSO-d_6,

Please cite this article in press as: X. Tian, et al., Double labelling of intracellular mitochondria and nucleolus using thiophene pyridium salt with high quantum yield as biosensor and its application in stimulated emission depletion nanoscopy, Analytica Chimica Acta (2017), https://doi.org/10.1016/j.aca.2017.12.033

400 MHz), δ (ppm): 8.65 (d, $J = 6.7$ Hz, 2H), 8.07 (d, $J = 15.7$ Hz, 1H), 7.98 (d, $J = 6.8$ Hz, 2H), 7.43 (t, $J = 7.9$ Hz, 4H), 7.30−7.19 (m, 7H), 6.73 (d, $J = 15.7$ Hz, 1H), 6.44 (d, $J = 4.1$ Hz, 1H), 4.14 (s, 3H). ^{13}C-NMR (100 MHz, DMSO-d_6), δ (ppm): 157.16, 152.60, 146.09, 144.31, 134.68, 133.95, 129.91, 129.61, 125.52, 124.63, 122.03, 117.70, 114.63, 46.37. IR (KBr, cm^{-1}) selected bands: 3448, 1644, 1590, 1529, 1491, 1455, 1430, 1310, 1212, 1190, 1150, 1055, 957, 834, 756, 739, 699, 618, 558, 537, 492. MALDI-TOF: *m*/*z*, cal: 514.11, found: 369.33 ([M-PF_6]$^+$).

MitoNuc2: Yield: 82%. Mp: 202 °C. ^{1}H-NMR (DMSO-d_6, 400 MHz), δ (ppm): 8.77 (d, $J = 6.7$ Hz, 2H), 8.13 (d, $J = 6.8$ Hz, 2H), 7.94 (d, $J = 16.2$ Hz, 1H), 7.62 (d, $J = 8.7$ Hz, 2H), 7.39 (m, 4H), 7.31 (d, $J = 16$ Hz, 1H), 7.13 (m, 6H), 6.95 (d, $J = 8.7$ Hz, 2H), 4.21 (s, 3H). ^{13}C-NMR (100 MHz, DMSO-d_6) δ (ppm): 152.79, 149.43, 146.17, 144.76, 140.48, 129.82, 127.94, 126.39, 125.37, 124.48, 122.87, 120.68, 120.43, 46.63. IR (KBr, cm^{-1}) selected bands: 2855, 1797, 1646, 1620, 1586, 1519, 1491, 1422, 1328, 1275, 1213, 1179, 1050, 984, 835, 752, 700, 620, 558, 538. MALDI-TOF: *m*/*z*, cal: 508.15, found: 363.18 ([M-PF_6]$^+$).

MitoNuc3: Yield: 73%, Mp:185 °C. ^{1}H-NMR (DMSO-d_6, 400 MHz), δ (ppm): 8.57 (d, $J = 6.8$ Hz, 2H), 8.03 (d, $J = 15.6$ Hz, 1H), 7.89 (d, $J = 6.8$ Hz, 2H), 7.28 (d, $J = 8.9$ Hz, 4H), 7.20 (d, $J = 4.2$ Hz, 1H), 6.98 (d, $J = 8.9$ Hz, 4H), 6.57 (d, $J = 15.6$ Hz, 1H), 6.10 (d, $J = 4.2$ Hz,1H), 4.11 (s, 3H), 4.03 (q, 4H), 1.33 (t, $J = 7.0$ Hz, 6H). ^{13}C-NMR (100 MHz, DMSO-d_6) δ (ppm): 160.58, 156.75, 152.81, 143.97, 138.66, 135.37, 135.14, 127.12, 126.59, 121.44, 115.60, 115.54, 109.38, 63.32, 46.12, 14.62. IR (KBr, cm^{-1}) selected bands: 3448, 2980, 1648, 1600, 1529, 1507, 1440, 1390, 1286, 1245, 1440, 1192, 1173, 1152, 1045, 959, 877, 838, 811, 717, 739, 659, 598, 557, 534. MALDI-TOF: *m*/*z*, cal: 602.16, found: 457.42 ([M-PF_6]$^+$).

MitoNuc4: Yield: 81%, Mp:183 °C. ^{1}H-NMR (DMSO-d_6, 400 MHz), δ (ppm): 8.72 (d, $J = 6.7$ Hz, 2H), 8.08 (d, $J = 6.7$ Hz, 2H), 7.89 (d, $J = 16.1$ Hz, 1H), 7.54 (d, $J = 8.8$ Hz, 2H), 7.12 (m, 5H), 6.95 (d, $J = 8.9$ Hz, 4H), 6.73 (d, $J = 8.8$ Hz, 2H), 4.19 (s, 3H), 4.02 (q, 4H), 1.33 (t, $J = 7.0$ Hz, 6H). ^{13}C-NMR (100 MHz, DMSO-d_6) δ (ppm): 155.98, 153.00, 150.64, 144.57, 140.95, 138.59, 129.68, 127.78, 125.73, 122.55, 119.01, 117.13, 115.60, 63.23, 46.50, 14.65. IR (KBr, cm^{-1}) selected bands: 2930, 2900, 2870, 1646, 1587, 1504, 1475, 1431, 1392, 1320, 1293, 1242, 1213, 1172, 1046, 1009, 981, 922, 840, 728, 674, 638, 603, 557, 541. MALDI-TOF: *m*/*z*, cal: 596.20, found: 451.23 ([M-PF_6]$^+$).

3. Results and discussion

3.1. Crystal structures

The crystal structures of **MitoNuc2-MitoNuc4** are displayed in Fig. 1, and crystallography data of **MitoNuc2-MitoNuc4** are summarized in Tables S1 and S2. As shown in Fig. 1, the dihedral angle between the pyridine ring and the benzene ring of **MitoNuc2** and **MitoNuc4** is 6.01° and 6.02°, respectively, which is smaller than that of **MitoNuc3** (the dihedral angle between the pyridine ring and the thiazole ring is 17.29°), indicating **MituNuc 2** and **MitoNuc4** are nearly coplanar. Meanwhile, all bond lengths in these three compounds, including C-C and C-N bands, are located in the range of the normal single and double bond. Moreover, the bond-length alternation (BLA) [32] across the π-bridge of **MitoNuc2-MitoNuc4** is 0.173 Å, 0.101 Å and 0.109 Å, respectively, indicating **MitoNuc3** possesses a high delocalization system within the molecule. All the data provide key parameters for good nonlinear optical properties of these thiophene pyridium derivatives.

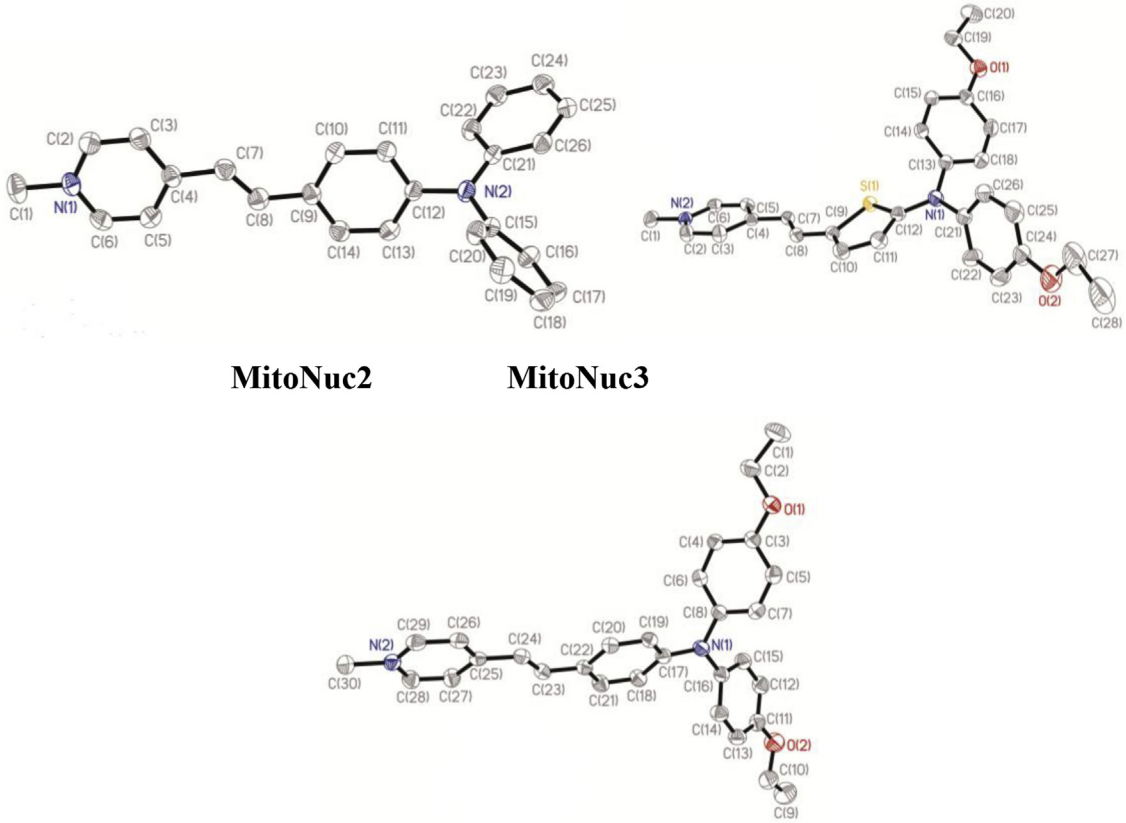

Fig. 1. Crystal structures of **MitoNuc2-MitoNuc4**. All H atoms and PF_6^- ions are omitted for clarity.

Please cite this article in press as: X. Tian, et al., Double labelling of intracellular mitochondria and nucleolus using thiophene pyridium salt with high quantum yield as biosensor and its application in stimulated emission depletion nanoscopy, Analytica Chimica Acta (2017), https://doi.org/10.1016/j.aca.2017.12.033

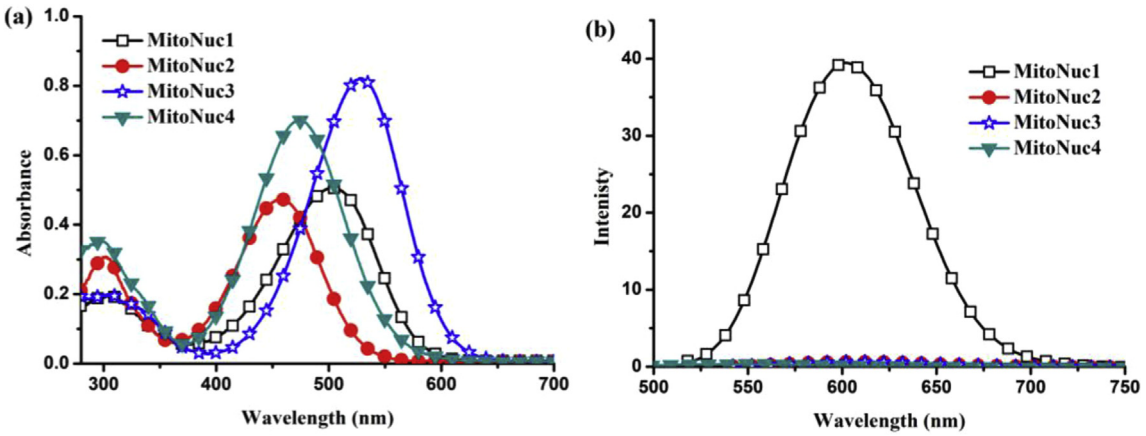

Fig. 2. (a) UV-*vis* absorption and (b) one-photon fluorescence spectra of **MitoNuc1-MitoNuc4** in PBS buffer.

3.2. Photophysical properties

The photophysical properties of **MitoNuc1**-**MitoNuc4** in different solvents were depicted in Figs. S2–S3, and the corresponding data are listed in Table S3. From Fig. S2, it can be seen that **MitoNuc1**-**MitoNuc4** exhibited two absorption bands. The higher energy band was assigned to the π-π* transition of triphenylamine/diphenylamine thiophene group, respectively, while the lower energy band can be assigned to intramolecular charge transfer (ICT). The results of theoretical calculations were carried out, which were well consistent with the experimental results (Fig. S4 and Table S4). Moreover, the maximum absorption bands of the compounds (Fig. 2a) exhibited a red-shift in the order of **MitoNuc2** < **MitoNuc4** < **MitoNuc1** < **MitoNuc3**, resulting from the increased electron-donating strength of the terminal group. The water solubility of **MitoNuc1-MitoNuc4** was also investigated (Fig. S5). The linear absorption behavior confirmed that all the compounds possessed good water solubility in concentration range of 2–50 μM. There is only a small structural difference between the compounds **MitoNuc1**, **MitoNuc2** and **MitoNuc3**, **MitoNuc4**, but there are large differences in their spectral characters. From Table S3, the fluoresce band of **MitoNuc3** are red-shifted relative to **MitoNuc1**. This spectral-shift may be attributed that the N, N-bis(4-ethoxyphenyl) aniline group as a donor is stronger than the diphenylamine thiophene group, owing to delocalization of the π electrons onto the N, N-bis(4-ethoxyphenyl)aniline. However, the quantum yield of **MitoNuc3** is lower than that of **MitoNuc1** (Fig. 2b), which is explained that the stronger donor and acceptor group may cause

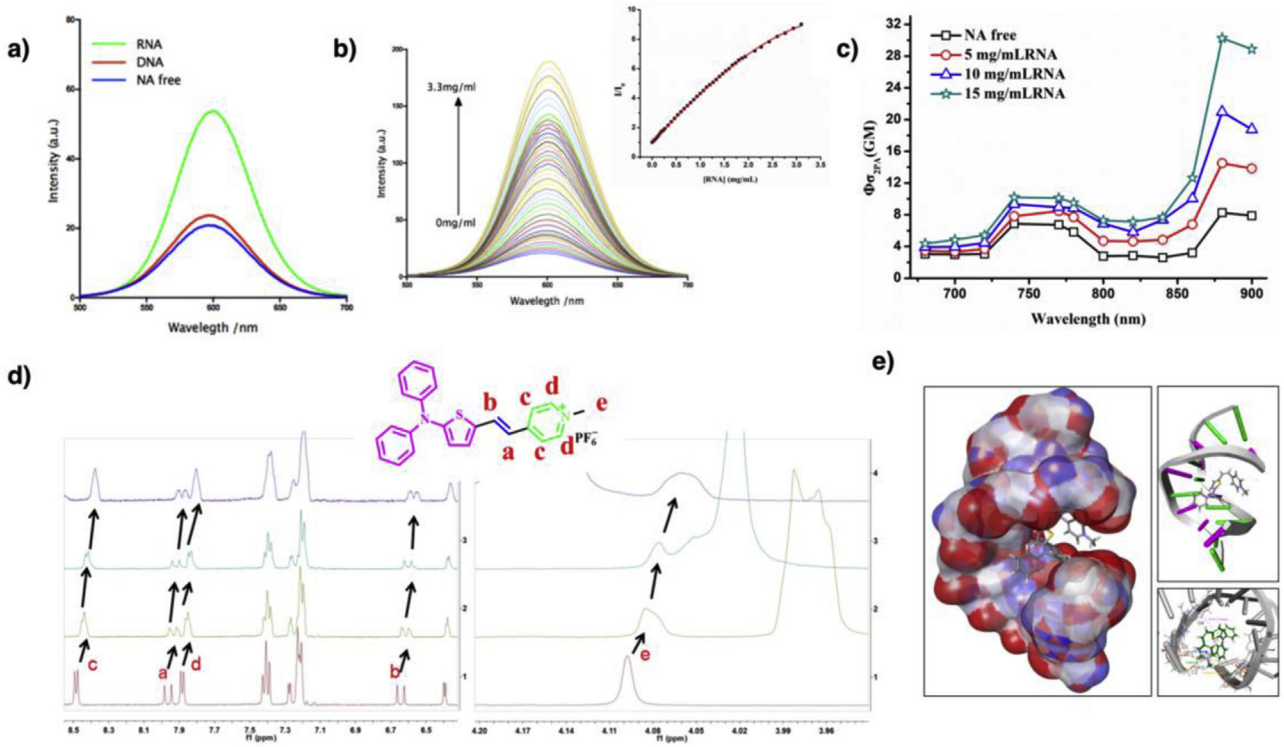

Fig. 3. a) The fluorescence enhancement of **MitoNuc1**with0.2 mg/mL DNA and RNA, respectively. b) The fluorescence spectra of **MitoNuc1**withthe addition of RNA (0–3.33 mg/mL). Inset: fluorescence titrations curve of 10 μM **MitoNuc1** by different concentration of RNA. c) Two-photon action cross-section values of **MitoNuc1** with RNA. d) Partial ^{1}H NMR titration spectra for **MitoNuc1**+ RNA for in DMSO-d6/D_2O (v/v, 5:1). e) The molecular docking between RNA and **MitoNuc1.**

Please cite this article in press as: X. Tian, et al., Double labelling of intracellular mitochondria and nucleolus using thiophene pyridium salt with high quantum yield as biosensor and its application in stimulated emission depletion nanoscopy, Analytica Chimica Acta (2017), https://doi.org/10.1016/j.aca.2017.12.033

the energy loss in the excited state vibration to quench the fluorescence resulting in the lower fluorescence quantum yield [33]. The Stokes shifts of **MitoNuc1-MitoNuc4** were about 110 nm, 137 nm, 96 nm and 77 nm, respectively, which offer more advantages over commercial organic cellular dyes, such as Mitotracker Red CMXRos and SYTO 9 (Stokes shift = 20 and 15 nm, respectively). Noteworthy that although it is out of current study scope, the two-photon cross-section values (σ) of **MitoNuc1- MitoNuc4** were measured by Z-scan method. From Fig. S6, it can be seen that the σ show the sequence: **MitoNuc2** (205 GM) < **MitoNuc4** (379 GM) < **MitoNuc1** (410 GM) < **MitoNuc3** (616 GM), which can be explained by the fact that increase the electron density of the bridge, favoring the ICT along the extended π-bridge from terminal donor to acceptor group. Comparing the other derivatives, **MitoNuc1** has a moderate σ value, as well as higher quantum yields, which stimulated us to further explore its potential application for mitochondria and nucleolus double labeling purpose.

3.3. Binding affinity of MitoNuc1 and molecular docking with RNA in vitro

According to the initial design purpose, the interactions of **MitoNuc1** with DNA and RNA were studied by one-photon fluorescence spectroscopy. From Fig. 3a, by the addition of 0.2 mg/mL DNA or RNA, the fluorescence intensity of **MitoNuc1** exhibited an approximately 1.15-fold and 2.65-fold enhancement in the presence of DNA and RNA, respectively. The result indicated that **MitoNuc1** has a better interaction with RNA than DNA. The mechanism of the light-up effect of **MitoNuc1** binding to RNA could be explained by two factors. Firstly, **MitoNuc1** is protected from water in the hydrophobic environment offered by the higher-order structure of RNA. Secondly, the torsional motion of vinyl groups may be restricted by the steric effect derived from the interactions between the cationic N-pyridinium unit and the anionic phosphate of RNA. The fluorescence intensity of **MitoNuc1** at 599 nm was increased 8.7-fold when the concentration of RNA was

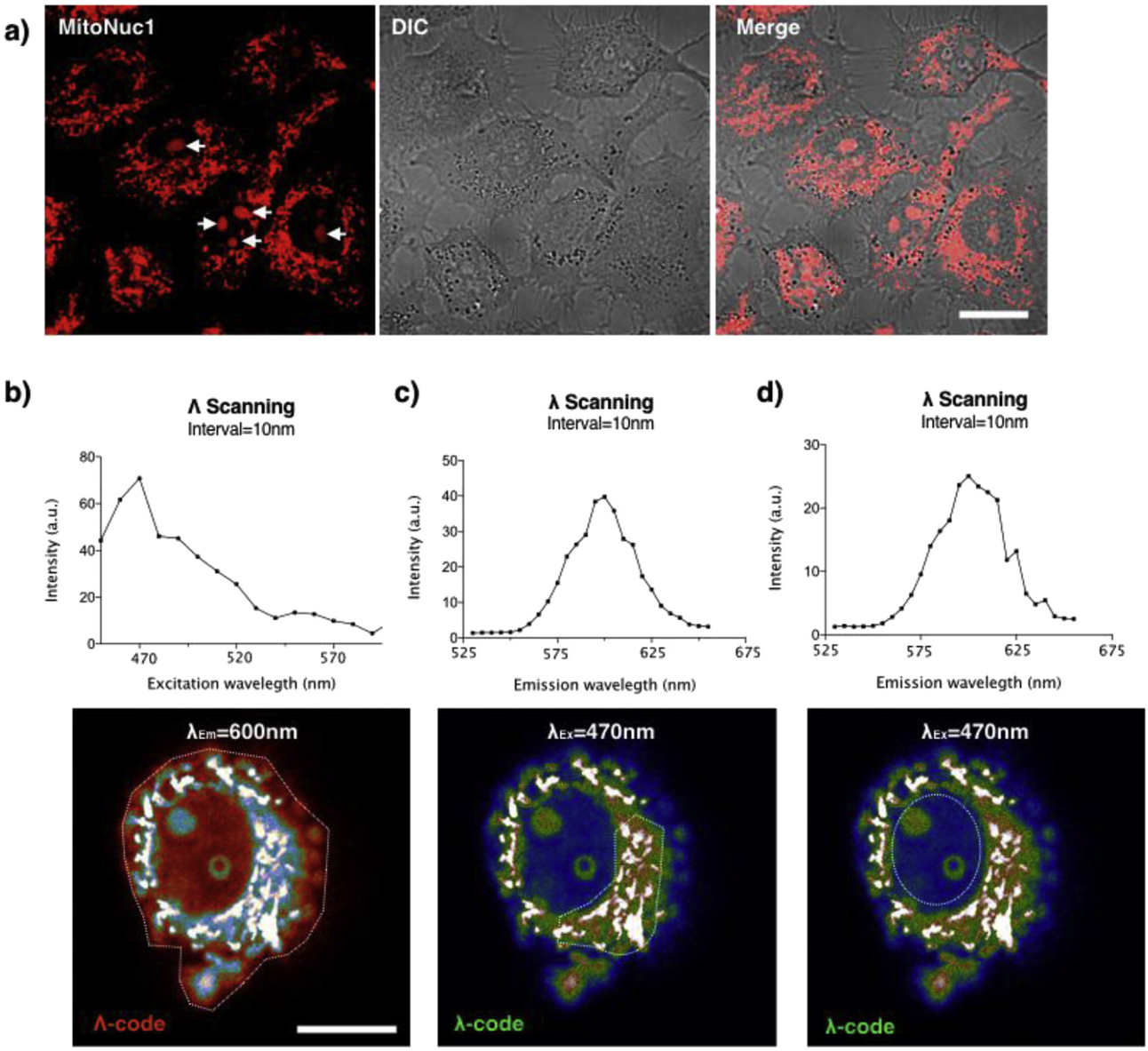

Fig. 4. a) Confocal micrographs using HepG2 cells incubated with **MitoNuc1**compound and merged with DIC channel, the white arrow indicates nucleolus. b) Λ scanning experiments to determine the *in cellulo* excitation wavelength of **MitoNuc1**. λ-scanning experiments to determine the *in cellulo* emission wavelength from c) cytosolic region and d) nuclear region. Scale bar = 10 μm.

Please cite this article in press as: X. Tian, et al., Double labelling of intracellular mitochondria and nucleolus using thiophene pyridium salt with high quantum yield as biosensor and its application in stimulated emission depletion nanoscopy, Analytica Chimica Acta (2017), https://doi.org/10.1016/j.aca.2017.12.033

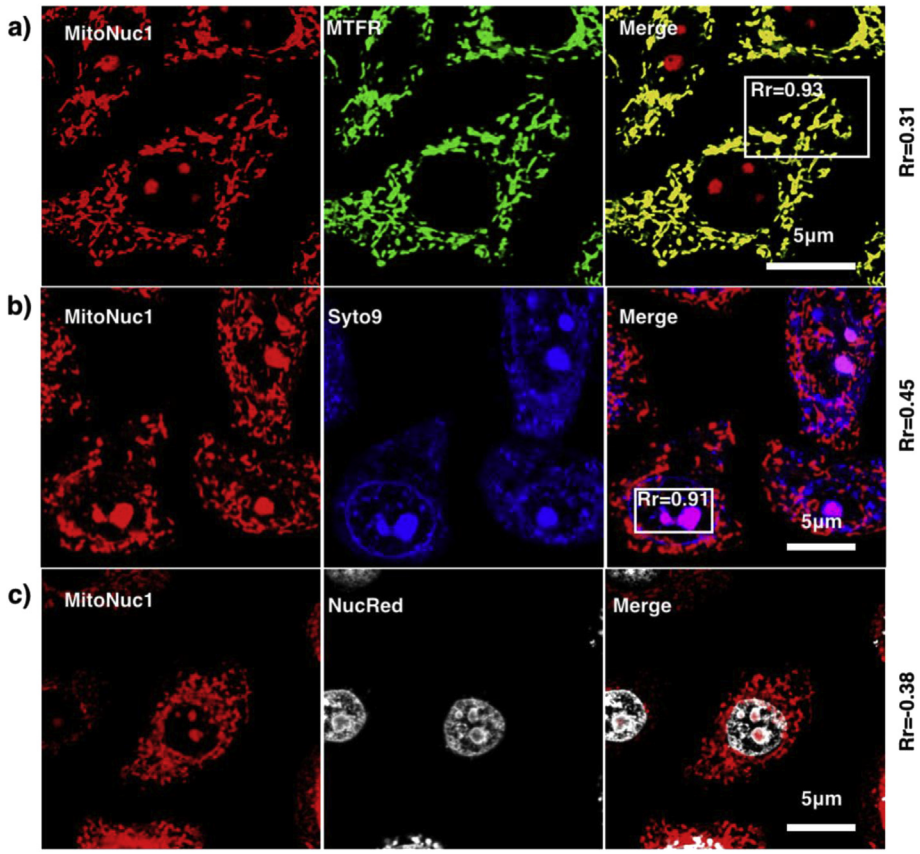

Fig. 5. Colocolization experiments using HepG2 cells incubated with **MitoNuc1**compound and co-stained with a) Mitotracker Far-Red b) Syto-9 and c) Nuc-Red. (For interpretation of the references to colour in this figure legend, the reader is referred to the Web version of this article.)

increased from 0 to 3.33 mg/mL (Fig. 3b), as well as the association constant $K = 2.67 \times 10^4\ M^{-1}$ The response of **MitoNuc1** to various amino acids, DNA, RNA and proteins was further investigated to demonstrate the selectivity of **MitoNuc1** towards RNA. **MitoNuc1** was treated with various amino acids (Ala, Trp, Ser, Glu, GSH, His, Cys, Hcy, Lys.), DNA, RNA and proteins (BSA, HSA). From Fig. S7, the fluorescence intensity of **MitoNuc1** was strongly increased with the addition of RNA, no fluorescence response occurred for amino acids and proteins. The competition experiment was also carried out by RNA to the solution of **MitoNuc1** in the presence of the amino acids, DNA and proteins. As displayed in Fig. S7, an obvious fluorescence changes were observed for **MitoNuc1** upon addition of RNA, suggesting that these commonly coexisting amino acids and proteins do not interfere in "off-on" fluorescent response for RNA. The effect of pH and ionic strength for **MitoNuc1** in the absence or presence of RNA was investigated by fluorescence spectra changes. From Fig. S8, **MitoNuc1** was stable in a pH region of 6–8, while the fluorescence intensity of **MitoNuc1** exhibited no obvious changes with the increasing concentration of NaCl. From Fig. 3c, the maximum two-photon action cross-section at 880 nm of **MitoNuc1** showed an approximately 3.75-fold enhancement with bonding to RNA. Its reasonable two-photon action cross-sections are the attractive features for their utility as bioimaging probes. Compare to the other three compounds as shown in Fig. 3a and Fig. S9, **MitoNuc3** exhibited a stronger interaction with RNA than **MitoNuc2** and **MitoNuc4**. Moreover, **MitoNuc1** showed a better interaction with RNA than **MitoNuc3**. To further confirm that **MitoNuc1**was encapsulated by RNA, ^{1}H NMR titration experiments were carried out in DMSO-d6/D_2O (v/v, 5:1). As shown in Fig. 3d, the addition of RNA generated significant upfield shifts of the olefin protons H_a-H_b and the 4-methyl pyridine protons H_c - H_e. The results demonstrated that it maybe exist hydrogen bonds and π-π stacking interactions between terpyridine fragments of **MitoNuc1** and RNA. Such *in vitro* results of **MitoNuc1-MitoNuc4** were further strengthened *via* molecular modeling calculations using Discovery Studio 4.1 with duplex GC riched RNA fragment (ID: 5TDK, CCGGCGCCGG/CCGGCGCCGG, retrieved from PDB database [34]). As shown in Fig. 3e and Fig. S10, **MitoNuc1** exhibited clear insert into RNA and its detailed interactions including hydrogen bonds and π•••π stacking were also displayed. Although **MitoNuc2**, **MitoNuc3 and MitoNuc4** also demonstrated possible binding with RNA (Figs. S11–S13), while the required binding energy was clearly higher than that of **MitoNuc1** (**MitoNuc1**: −397.225, **MitoNuc2**: −345.547, **MitoNuc3**: −323.160, **MitoNuc4**: −294.160, Unit: kcal/mol, Table S5), suggesting **MitoNuc1** might have the best spatial structure for RNA labeling. The above computational results were also in agreement with later *in cellulo* work that **MitoNuc1** was the only compound capable for efficient nucleolar binding.

3.4. *In cellulo photophysical properties and intracellular distribution*

To evaluate **MitoNuc1** uptake in living cells, HepG2 cells (human liver carcinoma cells) were used as a model and incubated with **MitoNuc1** (5 μM) for 30 min (37 °C, 5% CO_2). Prior to this low toxicity of **MitoNuc1** has been confirmed (Fig. S14). Due to its good water solubility and small molecular weight, sufficient signals were clearly observed under confocal microscopy ($\lambda_{ex} = 488$ nm, $\lambda_{em} = 600$–650 nm) throughout the cells that suggested effective

Please cite this article in press as: X. Tian, et al., Double labelling of intracellular mitochondria and nucleolus using thiophene pyridium salt with high quantum yield as biosensor and its application in stimulated emission depletion nanoscopy, Analytica Chimica Acta (2017), https://doi.org/10.1016/j.aca.2017.12.033

uptake within short incubation period. Furthermore, differential interference contrast (DIC) channel revealed good cell shape after internalization, in agreement with the initial MTT assay that suggested the minimal invasiveness of **MitoNuc1** compounds (Fig. 4a). It is noteworthy that both cytosolic and nuclear regions emitted strong luminescence, while the former displaying elongated and random fibril structure, the latter was observed circular punctate pattern around ~0.5–1.0 μm (white arrow).

To confirm the *in cellulo* photophysical properties of **MitoNuc1** compound, confocal equipped with White-Laser (adjustable excitation source from 460 nm to 700 nm) was used; Λ and λ-Scanning experiments were performed to determine the *in situ* excitation and emission across a range of wavelengths for a single emission (or excitation), respectively (Fig. 4b–d). As shown in Fig. 4b, once the whole cells were chosen and the emission was fixed at 600 nm, maximal excitation laser (λ = 420–590 nm, interval = 10 nm) could be found at ~ 470 nm, similarly as obtained *in vitro*. As the excitation was fixed at 470 nm, clearly either from cytosolic region (Fig. 4c) or nuclear signal (Fig. 4d), its emission peak was located at ~ 600 nm, which was again in agreement with the spectrum found in solvent. The Λ and λ-Scanning experiments suggested the photophysical properties of **MitoNuc1** including excitation and emission wavelengths remained unchanged upon intracellular internalization.

3.5. Intracellular colocolization study of MitoNuc1

To examine the precise subcellular compartments that **MitoNuc1** targeted, a series of colocolization experiments were performed. As showed in Fig. 5a, the cytosolic **MitoNuc1** signal demonstrated perfect overlapping with MitoTracker Far-Red (MTFR, $\lambda_{ex} = 633$ nm, $\lambda_{em} = 650–670$ nm), a commercial dye that specifically stain intracellular mitochondria. This is not unexpected; since pyridium based molecular system tend to target living cell mitochondria with high membrane potential. In parallel, a nucleic acid dye Syto9 ($\lambda_{ex} = 488$ nm, $\lambda_{em} = 500–520$ nm), which stains the cytosolic and nucleolar RNA of living cells, displayed clear coincidence with **MitoNuc1** at nuclear region, whereas the cytosolic signal of Syto9 indicated few association (Fig. 5b). This highly suggested that as same as Syto9, the binding source of **MitoNuc1** compound within nucleus is RNA. Conversely, colocolization using a DNA commercial stain NucRed ($\lambda_{ex} = 633$ nm, $\lambda_{em} = 650–670$ nm) was also performed and displayed a clear different nuclear distribution pattern (Fig. 5c), as no signal was observed from chromatin place but from nucleolar region, suggesting that the **MitoNuc1** compound was preferentially bound RNA over DNA at nucleus. Notably, although extensive RNA species were existed in cytosol as highlighted *via* Syto9 dye, **MitoNuc1** compound tends to accumulate on mitochondrial sites due to its cationic nature. The high affinity of **MitoNuc1** against RNA could only play such role once it permeates the nuclear envelope and internalizes within nucleolus. Interestingly it was observed that **MitoNuc2**, **MitoNuc3 and MitoNuc4** possessing bigger molecular weight displayed weak nucleolar binding and unspecific cytosolic distribution (Fig. S15).

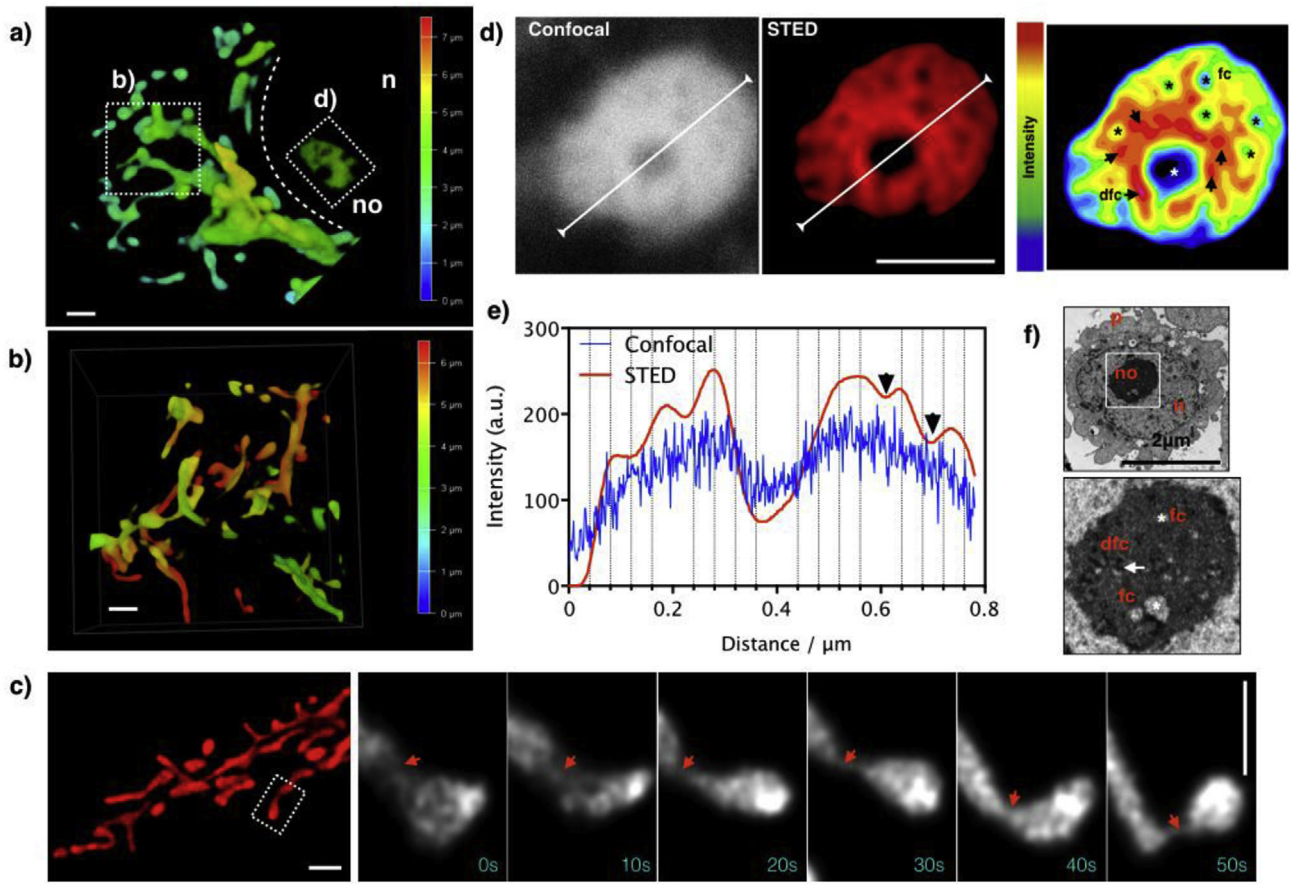

Fig. 6. STED images using HepG2 cells incubated with **MitoNuc1**compound. a) 3D re-construction of magnified cell comprised with mitochondria and nucleoli. b) 3D re-construction of magnified mitochondrial sections from selected region from a). c) Real-time STED images displayed mitochondrial division. d) Comparison of confocal and STED images of single nucleoli with its fluorescent intensity map. e) Fluorescent intensity profile of single nucleoli at d). f) Correspondence EM micrographs also indicated nucleolar ultrastructure. Scale bar = 1 μm. No, p, fc and dfc represent nucleolus, plasma membrane and fibril centre and dense fibril centre, respectively.

Please cite this article in press as: X. Tian, et al., Double labelling of intracellular mitochondria and nucleolus using thiophene pyridium salt with high quantum yield as biosensor and its application in stimulated emission depletion nanoscopy, Analytica Chimica Acta (2017), https://doi.org/10.1016/j.aca.2017.12.033

3.6. Application in stimulated emission depletion nanoscopy

The successful double staining of mitochondria and nucleolus using **MitoNuc1** showed stable fluorescence and reasonable brightness using low molar weight (working concentration = 5 μm). We therefore were further motivated to push its imaging utilization under stimulated emission depletion (STED) nanoscopy in living cells. A STED micrograph of **MitoNuc1** incubated cells comprising partial nuclear region and associated mitochondria in 3-Dimensional (3D) was firstly captured (Fig. 6a). Apparently complex mitochondrial network and nucleolar structures were displayed with high signal-to-noise ratio. Furthermore, magnified region selected from Fig. 4a showed granular, flat or line shaped mitochondrial structures in living cells (Fig. 6b). To examine **MitoNuc1** capability of mitochondrial labelling in dynamic manner under STED, a xyt (real-time) experiment was performed. From selected region of Fig. 6b, we successfully captured an ultrastructure that underwent mitochondrial division, from an integrated wire-like structure to a granular structure. Noteworthy, such division/fusion over time in high-resolution as obtained above is considered as a key process that how mitochondrial regulate their morphology, subsequently assign to different intracellular function. Whereas the actual mechanism is still remaining largely unclear, thus **MitoNuc1** compounds might offer a tool to study related process. Eventually, **MitoNuc1** stained nucleolar micrograph under STED was also successfully taken (Fig. 6d). Compared with magnified confocal microscopy, **MitoNuc1** again displayed superb signal-to-noise ratio (Fig. 6e). Notably, clear fibrillar centre (fc, star, RNA-rich) and dense fibrillar component (dfc, arrow, DNA-rich) ultrastructure were obtained (Fig. 6d, intensity map), and similarly shaped fc patches were also seen in a parallel transmission electron microscopy (TEM) experiment (Fig. 6f). This again suggested that **MitoNuc1** possesses higher affinity towards RNA than DNA, thus might offer a fascinating tool to study nucleolar ultrastructure in dynamic manner in living cells.

4. Conclusion

In conclusion, four pyridine salt derivatives (**MitoNuc1-4**) were designed and confirmed crystallographically. It was found that compound **MitoNuc1** containing thiophene bridge possessed good biocompatibility, suitable quantum yield, large two-photon absorption cross-sections in the near infrared region, and small molecular weight. We demonstrated unique double labelling phenomena in living cells and proved the targeting compartments were mitochondria and nucleolus. Such intrigued results could be supported by both *in vitro* and molecular docking experiments. Further contribution using **MitoNuc1** as an imaging tool in living cells under STED nanoscopy successfully showed super resolution mitochondria and nucleolus ultrastructure in 3D and real-time manner. It is anticipated that such small molecular system could not only provide *in cellulo* imaging probes, but also offer an idea how to design tools for multi-organelle targeting.

Acknowledgement

This work was supported by grants from the National Natural Science Foundation of China (21602003, 51432001, 51672002 and 51372003), Anhui Provincial Natural science foundation of China (1708085MC68), and Anhui University Doctor Startup Fund (J01001962).

Appendix A. Supplementary data

Supplementary data related to this article can be found at https://doi.org/10.1016/j.aca.2017.12.033.

References

[1] E.L. Que, D.W. Domaille, C.J. Chang, Chem. Rev. 108 (2008) 1517.
[2] T. Ueno, T. Nagano, Nature methods 8 (2011) 642.
[3] H.M. Kim, B.R. Cho, Chem. Rev. 115 (2015) 5014.
[4] L. Schermelleh, R. Heintzmann, H. Leonhardt, J. Cell Biol. 190 (2010) 165.
[5] M. Bates, B. Huang, G.T. Dempsey, X. Zhuang, Science 317 (2007) 1749.
[6] V. Westphal, S.O. Rizzoli, M.A. Lauterbach, D. Kamin, R. Jahn, S.W. Hell, Science 320 (2008) 246.
[7] B. Hein, K.I. Willig, S.W. Hell, Proc. Natl. Acad. Sci. Unit. States Am. 105 (2008) 14271.
[8] D. Li, L. Shao, B.-C. Chen, X. Zhang, M. Zhang, B. Moses, D.E. Milkie, J.R. Beach, J.A. Hammer, M. Pasham, Science 349 (2015) aab3500.
[9] J.D. Bryngelson, J.N. Onuchic, N.D. Socci, P.G. Wolynes, Proteins: Structure, Function, and Bioinformatics 21 (1995) 167.
[10] H. Lodish, D. Baltimore, A. Berk, S.L. Zipursky, P. Matsudaira, J. Darnell, Molecular Cell Biology, vol. 3, Scientific American Books New York, 1995.
[11] L. Yuan, W. Lin, K. Zheng, S. Zhu, Accounts Chem. Res. 46 (2013) 1462.
[12] R. Aloya, A. Shirvan, H. Grimberg, A. Reshef, G. Levin, D. Kidron, A. Cohen, I. Ziv, Apoptosis 11 (2006) 2089.
[13] Q. Wan, S. Chen, W. Shi, L. Li, H. Ma, Angew. Chem. Int. Ed. 53 (2014) 10916.
[14] Z. Liu, F. Hao, H. Xu, H. Wang, J. Wu, Y. Tian, CrystEngComm 17 (2015) 5562.
[15] Y. Tang, H. Liu, H. Zhang, D. Li, J. Su, S. Zhang, H. Zhou, S. Li, J. Wu, Y. Tian, Spectrochim. Acta Mol. Biomol. Spectrosc. 175 (2017) 92.
[16] Y. Niko, H. Moritomo, H. Sugihara, Y. Suzuki, J. Kawamata, G.-i Konishi, J. Mater. Chem. B 3 (2015) 184.
[17] G. Zhang, Y. Sun, X. He, W. Zhang, M. Tian, R. Feng, R. Zhang, X. Li, L. Guo, X. Yu, Anal. Chem. 87 (2015) 12088.
[18] Q. Zhang, X. Tian, H. Zhou, J. Wu, Y. Tian, Materials 10 (2017) 223.
[19] N. Kumar, V. Bhalla, M. Kumar, Chem. Commun. 51 (2015) 15614.
[20] D. Li, X. Tian, A. Wang, L. Guan, J. Zheng, F. Li, S. Li, H. Zhou, J. Wu, Y. Tian, Chem. Sci. 7 (2016) 2257.
[21] D. Li, D. Yu, Q. Zhang, S. Li, H. Zhou, J. Wu, Y. Tian, Dyes Pigments 97 (2013) 278.
[22] D. Li, Q. Zhang, X. Sun, N. Shao, R. Li, S. Li, H. Zhou, J. Wu, Y. Tian, Dyes Pigments 102 (2014) 79.
[23] F. Hao, X. Zhang, Y. Tian, H. Zhou, L. Li, J. Wu, S. Zhang, J. Yang, B. Jin, X. Tao, J. Mater. Chem. 19 (2009) 9163.
[24] M.R. Harpham, O.z.n. Süzer, C.-Q. Ma, P. Bäuerle, T. Goodson III, J. Am. Chem. Soc. 131 (2009) 973.
[25] J. Tan, R. Li, D. Li, Q. Zhang, S. Li, H. Zhou, J. Yang, J. Wu, Y. Tian, Dalton Trans. 44 (2015) 1473.
[26] A. Wojciechowski, M.M.M. Raposo, M.C.R. Castro, W. Kuznik, I. Fuks-Janczarek, M. Pokladko-Kowar, F. Bureš, J. Mater. Sci. Mater. Electron. 25 (2014) 1745.
[27] I.F. Perepichka, D.F. Perepichka, Handbook of Thiophene-based Materials: Applications in Organic Electronics and Photonics, 2 Volume Set, John Wiley & Sons, 2009.
[28] M. Zhao, J. Tan, J. Su, J. Zhang, S. Zhang, J. Wu, Y. Tian, Dyes Pigments 130 (2016) 216.
[29] J. Tan, Y. Zhang, M. Zhang, X. Tian, Y. Wang, S. Li, C. Wang, H. Zhou, J. Yang, Y. Tian, J. Wu, J. Mater. Chem. C 4 (2016) 3256.
[30] H. Liu, L. Wu, F. Li, X. Wang, H. Pan, Y. Ni, J. Yang, S. Li, Y. Tian, J. Wu, Polyhedron 121 (2017) 53.
[31] X. Zhao, J. Liu, H. Wang, Y. Zou, S. Li, S. Zhang, H. Zhou, J. Wu, Y. Tian, Dalton Trans. 44 (2015) 701.
[32] H. Wang, Q. Zhang, J. Zhang, L. Li, Q. Zhang, S. Li, S. Zhang, J. Wu, Y. Tian, Dyes Pigments 102 (2014) 263.
[33] Q. Zhang, X. Tian, Z. Hu, C. Brommesson, J. Wu, H. Zhou, J. Yang, Z. Sun, Y. Tian, K. Uvdal, Dyes Pigments 126 (2016) 286.
[34] F. Shen, Z. Luo, H. Liu, R. Wang, S. Zhang, J. Gan, J. Sheng, Nucleic Acids Res. (2016) gkw1307.

Please cite this article in press as: X. Tian, et al., Double labelling of intracellular mitochondria and nucleolus using thiophene pyridium salt with high quantum yield as biosensor and its application in stimulated emission depletion nanoscopy, Analytica Chimica Acta (2017), https://doi.org/10.1016/j.aca.2017.12.033